

Article

Neural-Network-Based Terminal Sliding Mode Control of Space Robot Actuated by Control Moment Gyros

Xinhui Xia ¹, Yinghong Jia ^{1,*}, Xinlong Wang ¹ and Jun Zhang ^{2,3}¹ School of Astronautics, Beihang University, Beijing 100191, China² Beijing Institute of Control Engineering, Beijing 100190, China³ National Laboratory of Space Intelligent Control, Beijing 100190, China

* Correspondence: jia_yingh@163.com

Abstract: This paper studies the trajectory tracking control of a space robot system (SRS) in the presence of the lumped uncertainties with no prior knowledge of their upper bound. Although some related control methods have been proposed, most of them have either not been applied to SRSs or lack rigorous stability proof. Therefore, it is still a challenge to achieve high accuracy and rigorous theoretical proof for tracking control of SRSs. This paper proposes a new integrated neural network-based control scheme for the trajectory tracking of a SRS actuated by control moment gyros (CMGs). A new adaptive non-singular terminal sliding mode (ANTSM) control method is developed based on an improved radial basis function neural network (RBFNN). In the control method, a new weight update law is proposed to learn the upper bound of the lumped uncertainties. With the advantages of RBFNN and ANTSM, the controller has high control accuracy, fast learning speed and finite-time convergence. Different from most on-ground robotic manipulator controllers, a kinematic controller with position and attitude control laws is also designed for the satellite platform to remain stable. The stability of the closed-loop system is proved by the Lyapunov method with a high mathematical standard. Comparative simulation results demonstrate the effectiveness of the proposed control scheme with preferable performance and robustness.



Citation: Xia, X.; Jia, Y.; Wang, X.; Zhang, J. Neural-Network-Based Terminal Sliding Mode Control of Space Robot Actuated by Control Moment Gyros. *Aerospace* **2022**, *9*, 730. <https://doi.org/10.3390/aerospace9110730>

Academic Editor: Zhan Tu

Received: 31 August 2022

Accepted: 17 November 2022

Published: 19 November 2022

Publisher's Note: MDPI stays neutral with regard to jurisdictional claims in published maps and institutional affiliations.



Copyright: © 2022 by the authors. Licensee MDPI, Basel, Switzerland. This article is an open access article distributed under the terms and conditions of the Creative Commons Attribution (CC BY) license (<https://creativecommons.org/licenses/by/4.0/>).

Keywords: space robot; neural networks; integrated control; nonsingular terminal sliding mode; control moment gyros

1. Introduction

In recent decades, robotic systems have been playing an increasingly important role in space missions [1] such as refueling [2,3], repairing and cleaning up space debris [4–6]. SRSs are robotic systems made of a satellite platform (which is actuated by reaction wheels or thrusters) equipped with one or more robotic arms (which are generally actuated by joint motors). The strong dynamical coupling between the satellite platform and robotic arms as well as the strong uncertainty makes tracking control of SRSs extremely difficult [7]. Although a variety of control schemes have been well studied, it is still a challenge for high-accuracy tracking control of SRSs and its rigorous theoretical proof.

To reduce the strong dynamical coupling of SRSs, the reactionless actuation concept has achieved considerable applications, such as trajectory planning [8], momentum equalization controlling [9], and reactionless maneuvering [10]. The reactionless joint actuation concept was first proposed by Peck [11,12]. In the design concept, the manipulator links of robotic arms are connected by free revolute joints, while a scissored pair of CMGs is mounted on each link to actuate the system. Thus, the control torques are exerted directly on the robotic links, and the joint action/reaction torques are eliminated. Studies have shown that with the reactionless actuators, the peak attitude control torques can be reduced [13], and system-level pointing performance can be improved by reducing the disturbances created by robotic arms [14]. Therefore, to reduce the dynamical coupling of SRSs, CMGs are employed as manipulator link actuators in this paper.

Considering the strong lumped uncertainties including external disturbances and parameter uncertainties of SRSs, sliding mode control schemes with strong robustness have been studied widely [15,16]. However, the traditional sliding mode control of SRSs has two significant drawbacks. One potential drawback is that various assumptions about the upper bound of the lumped uncertainties have been made, which makes controllers limited. For example, the lumped uncertainties of SRSs are assumed to be bounded by a constant [17,18], a linear function of the state norm [19], or a polynomial function of the state norm with arbitrary given order [20,21]. Although controllers based on these assumptions are stable, these assumptions indeed limit the application of the controllers. Another significant drawback is that traditional sliding mode control can only achieve asymptotic convergence, which leads to infinite convergence time on the sliding mode, such as adaptive sliding mode control [22].

To overcome the drawbacks mentioned above, an improved finite-time sliding mode control method based on neural networks (NNs) was proposed. NNs are capable of estimating any nonlinear unknown functions with arbitrary accuracy without the prior knowledge of the upper bounds of uncertainties [23–25], such as Chebyshev NN (CNN) [26], radial basis function NN [27] and fuzzy NN [28]. Therefore, the aforementioned assumptions about the upper bounds of uncertainties are not needed in the sliding mode control based on NNs. On the other hand, compared with conventional sliding mode control, finite-time sliding mode control has the superiority of finite-time convergence, such as terminal sliding mode (TSM) control [29] and non-singular terminal sliding mode (NTSM) control [30,31]. In the finite-time tracking control method, a NTSM is normally proposed to steer configuration variables of robotic manipulators to the reference trajectories within an adjustable finite time [32,33]. Meanwhile, a combination of NNs and finite-time concepts is applied to applications of SRSs. Motivated by [34,35], neural-network-based finite-time sliding mode control is studied for a space robot in this paper.

Although some neural-network-based finite-time sliding mode control methods have been proposed in the past, most of them are applied to on-ground nonlinear systems, such as on-ground manipulator systems and general aircraft vehicles [36], and have not been applied to space robots. Vijay [37] proposed a back-stepping TSM controller using RBFNN for a three degrees of freedom (DOF) on-ground robotic manipulator. The TSM control law with an NN-based adaptive observer was developed for the precise trajectory tracking performance and enhanced disturbance rejection. However, the significant drawback was that singularity was not taken into account. TSM was also combined with RBFNN and fuzzy strategy for an on-ground robot manipulator system in [38] and [39] respectively. In the proposed methods, singularity was avoided by switching from TSM to linear sliding mode (LSM). Compared with NTSM control, this control scheme was more complicated. Zhang [35] proposed a NN-based fault tolerant controller via NTSM for an n-link on-ground robot manipulator with actuator failures. The method utilized Gaussian RBF to compensate for actuator failures and external disturbances. Guo [34] proposed an adaptive RBF-based NTSM controller for a joint-actuated space robot subject to unknown parameter uncertainties and external disturbances. However, the study was oriented to free-floating case ignoring the motion control of the platform. Xia [40] presented an ANTSM controller based on NNs for a space manipulator actuated by CMGs. It is worth mentioning that CMGs can only reduce but not completely eliminate the dynamic coupling between the platform and the manipulator. Thus, it is still necessary to consider the influence of the platform on the control accuracy of the manipulator. However, the motion of the platform was also neglected in [40]. The dynamical coupling between the platform and the manipulator was not discussed. The manipulator systems in the applications mentioned above are all on-ground systems, and the control algorithms cannot be applied to SRSs directly. Wang [41] investigated an adaptive learning control for SRSs using NNs. In the control method, NTSM and fast NTSM were used to design the robust control to achieve the fast realization of the desired trajectory. However, chattering problem was not considered in the controller design. Yan [42] focused on the chattering problem in the sliding mode control

and proposed low-chattering fixed-time NTSM controller for a free-floating space robot. However, the internal and external uncertainty of system was assumed to be bounded by a constant, which might limit the application of the controller. Therefore, an improved NN-based finite-time control scheme is required for SRSs with strong dynamical coupling and strong uncertainty to guarantee high accuracy, finite convergence and non-singularity.

Motivated by this requirement, this paper proposes a new integrated NN based non-singular finite time control scheme for a reactionless SRS actuated by CMGs. In the control method, an ANTSM trajectory tracking control based on RBFNN for space manipulators ensures finite time convergence and strong robustness with no prior knowledge of the upper bound of the system uncertainties. Ignoring the prior knowledge upper bound, the application range of the controller is expanded. Considering the dynamic coupling of the SRS, a kinematic controller for the satellite platform is also designed for stabilization. Finally, based on the ANTSM manipulator controller and the kinematic platform controller, a dynamics-based controller for the whole system is constructed. The stability of the system is proven using the Lyapunov method. The main contributions of this paper are summarized as follows:

1. CMGs are employed as reactionless manipulator actuators of a SRS to reduce the strong dynamic coupling between the platform and the manipulator.
2. A new integrated RBFNN-based non-singular finite control scheme is proposed for the SRS with lumped uncertainties. In the control method, a new weight update law applied to RBFNN is proposed. With the advantages of RBFNN and ANTSM, the controller has high control accuracy, fast learning speed and finite-time convergence. Compared with the traditional sliding mode control, the application range of the controller is extended by ignoring the upper bound of the lumped uncertainties.
3. Different from [34] and [40], the control method is applied to the space robot considering the position and attitude control of the satellite platform.
4. Rigorous theoretical proof is achieved by the Lyapunov method with a high mathematical standard. In the proof, the symbolic function is replaced by the saturation function to avoid the chattering problem for practical implementations.

This paper is organized as follows. Section 2 gives a description of the space robot system with a satellite platform and n manipulator links which are actuated by CMGs. Section 3 defines coordinate systems and formulates the SRS. In Section 4, an ANTSM trajectory tracking controller using an RBFNN with a new weight update law is proposed. Error convergence and robustness are discussed in detail. A kinematic controller for the platform and an inverse dynamic controller for the whole SRS are also designed in order to resist the remaining dynamic coupling and ensure preferable control accuracy. In Section 5, the closed-loop system with the proposed controllers is simulated. Section 6 involves a discussion of the conclusions.

2. System Description

Consider an SRS consisting of a satellite platform and a robotic manipulator, as shown in Figure 1. The SRS is viewed as a typical rigid multibody system constituted by $n + 1$ rigid bodies. Manipulator links are connected to each other through n single-DOF revolute joints, thus the SRS has $6 + n$ DOF.

For the sake of clarity, the SRS is denoted by one typical numbering method, in which the platform is denoted as B_0 , and manipulator links are denoted as B_1, B_2, \dots, B_n respectively. Link B_i connects with its inboard body $B_{c(i)}$ by the joint i . Each joint is driven by two identical single gimbal CMGs with the gimbal angles equal in magnitude but opposite in direction [43].

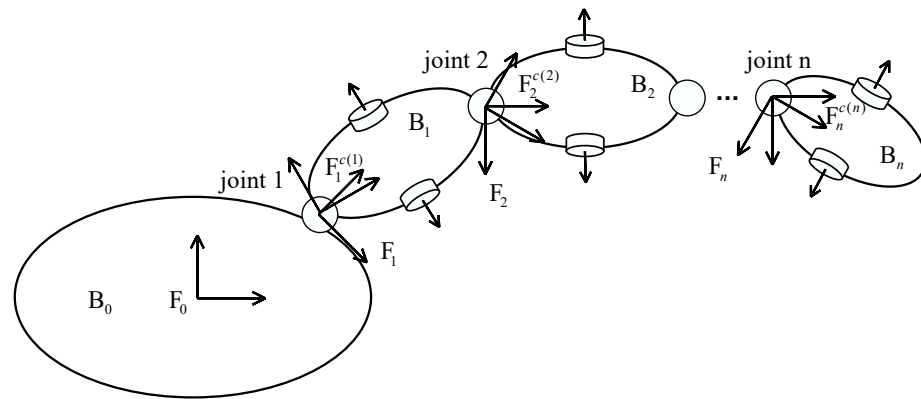


Figure 1. SRS with a satellite platform and a manipulator arm with CMG-actuation.

3. Equations of Motion

We formulate the equations of motion through an improved automatically generating algorithm based on Kane’s method which is proposed in Ref. [44] in detail. Reference frames are first introduced. The dynamic and kinematic equations are then derived for the SRS which are used for computer simulation.

3.1. Reference Frames

The inertial frame is denoted by \$F_e\$. A reference frame \$F_0\$ is attached to the platform \$B_0\$ as its body frame. \$F_0\$ can move with 6 DOF in the inertial frame. A body fixed frame \$F_i\$ is attached to \$B_i\$ and the origin of \$F_i\$ is located at the center of the \$i\$-th joint. An inboard body associated frame \$F_i^{c(i)}\$ is attached to \$B_{c(i)}\$. The origins of \$F_i\$ and \$F_i^{c(i)}\$ coincide

3.2. Dynamics Analysis

Consider a generalized displacement vector \$x \in R^{6+n}\$ and a generalized speed vector \$u \in R^{6+n}\$ which are introduced as

$$x = [r_b^T \quad \Theta_b^T \quad q^T]^T \tag{1}$$

$$u = [v_b^T \quad \omega_b^T \quad \dot{q}^T]^T \tag{2}$$

where \$r_b \in R^3\$ is defined as the position vector from \$F_e\$ to \$F_0\$ expressed in \$F_e\$, \$\Theta_b \in R^3\$ is the Euler angle vector of \$F_0\$ relative to \$F_e\$, \$v_b \in R^3\$ and \$\omega_b \in R^3\$ are the linear and angular velocities of \$F_0\$ with respect to \$F_e\$, respectively. \$q = [q_1 \quad q_2 \quad \dots \quad q_n]^T \in R^n\$ is the vector of joint angles, whose item \$q_i (i = 1, 2, \dots, n)\$ is the relative rotational angle between \$B_i\$ and \$B_{c(i)}\$.

Based on the definition of the generalized displacement \$x\$ and the generalized speed \$u\$, the dynamics of a CMG-driven \$n\$-joint rigid space manipulator system can be described by the following second-order nonlinear differential equation using Kane’s equations [45,46]

$$M(x)\dot{u} + F^{lt}(x, u) = F^A + T_d \tag{3}$$

where \$M(x) \in R^{(6+n) \times (6+n)}\$ is the symmetric positive mass matrix, \$F^{lt}(x, u) \in R^{6+n}\$ is the system nonlinear generalized inertia forces, \$F^A \in R^{6+n}\$ is the system generalized active forces and \$T_d \in R^{6+n}\$ is the external disturbance forces/torques. To simplify notation, \$M(x)\$ is simply written as \$M\$ and \$F^{lt}(x, u)\$ is simply written as \$F^{lt}\$ in the following.

According to Kane’s method, \$M\$ and \$F^{lt}\$ are contributed to by all the bodies in the space manipulator system through the following superposition equations

$$M = \sum_{i=0}^n M_i, F^{lt} = \sum_{i=0}^n F_i^{lt} \tag{4}$$

where M_i and F_i^{It} are the contributions of B_i to M and F^{It} , respectively. M_i and F_i^{It} can be calculated by the following two higher order nonlinear equations:

$$M_i = {}^p v_i^T (m_i {}^p v_i - s_i \times {}^p \omega_i) + {}^p \omega_i^T (s_i \times {}^p v_i + I_i {}^p \omega_i) \quad (i = 0, 1, \dots, n) \tag{5}$$

$$F_i^{It} = {}^p v_i^T [m_i \dot{v}_{it} - s_i \times \dot{\omega}_{it} + \omega_i \times \omega_i \times s_i] + {}^p \omega_i^T [s_i \times \dot{v}_{it} + I_i \dot{\omega}_{it} + \omega_i \times I_i \omega_i] \quad (i = 0, 1, \dots, n) \tag{6}$$

Therein, the superscript “ \times ” indicates the cross-product matrix of a 3×1 column matrix. m_i , s_i , I_i and ω_i are the mass, static moment, inertial dyadic and angular velocity of B_i . ${}^p v_i \in \mathbb{R}^{3 \times (6+n)}$ and ${}^p \omega_i \in \mathbb{R}^{3 \times (6+n)}$ are the partial velocity matrix and the partial angular velocity matrix of B_i , respectively. $v_{it} \in \mathbb{R}^3$ and $\omega_{it} \in \mathbb{R}^3$ are the nonlinear parts of the inertial velocity $v_i \in \mathbb{R}^3$ and angular velocity $\omega_i \in \mathbb{R}^3$ of B_i . The relationship between the inertial or angular velocity and the four kinematics quantities mentioned above can be easily obtained according to Maggi-Kane’s method.

For a common space manipulator system, there are external forces $f_b \in \mathbb{R}^3$ and torques $\tau_b \in \mathbb{R}^3$ applied to the platform and internal torques $\tau_m \in \mathbb{R}^n$ on the revolute joints. The generalized active forces of the system F^A are the sum of contributions over all the rigid bodies. It is worth mentioning that the internal torques generated by CMGs can be calculated by the following equation

$$\tau_m = -H - B\dot{h} \tag{7}$$

where $H \in \mathbb{R}^n$ is the torque caused by changes of the direction of the angular momentum of CMGs $h = [h_1 \ h_2 \ \dots \ h_n]^T \in \mathbb{R}^n$, $B \in \mathbb{R}^{n \times n}$ is the control torque gain caused by changes of the magnitude of h . H and B can be expressed by the following equations

$$H = \sum_{i=1}^n ({}^p \omega_i^m)^T \omega_i \times \Gamma_i h_i \tag{8}$$

$$B = [({}^p \omega_1^m)^T \Gamma_1 \quad ({}^p \omega_2^m)^T \Gamma_2 \quad \dots \quad ({}^p \omega_n^m)^T \Gamma_n] \tag{9}$$

where ${}^p \omega_i^m \in \mathbb{R}^{3 \times n}$ is the last n columns of the partial angular velocity matrix ${}^p \omega_i$. $\Gamma_i (i = 1, 2, \dots, n)$ is the projection of the unit vector along the rotation axes and only the component of the corresponding rotation axis of the i -th joint is 1.

In real cases, both the platform and manipulators could be affected by external perturbations. However, in the present it is reasonable to assume that no external disturbance forces/torques act on the platform, since the mass of the platform is great enough and external forces/torques acting upon the platform are usually small and can be ignored. The external disturbance torques of manipulator joints are defined as $\tau_d \in \mathbb{R}^n$, and then the external disturbance forces/torques T_d in Equation (3) can be described as follows

$$T_d = [0_{3 \times 1}^T \quad 0_{3 \times 1}^T \quad \tau_d^T]^T \tag{10}$$

Substituting Equations (2), (7) and (10) into Equation (3), the dynamic equations of the space manipulator system can be rewritten as

$$M \begin{bmatrix} \dot{v}_b \\ \dot{\omega}_b \\ \ddot{q} \end{bmatrix} + F^{It} = \begin{bmatrix} f_b \\ \tau_b \\ -H - B\dot{h} \end{bmatrix} + \begin{bmatrix} 0 \\ 0 \\ \tau_d \end{bmatrix} \tag{11}$$

3.3. Kinematics Analysis

It can be seen from Equations (5) and (6) that M_i and F_i^{It} can be calculated by five kinematics quantities ${}^p v_i$, ${}^p \omega_i$, ω_i , v_{it} and ω_{it} . The five kinematics quantities can be obtained through a recursive procedure.

Consider a generic manipulator link $B_i (i = 1, 2, \dots, n)$ and its inboard body $B_{c(i)}$ connected by real joint i . The recursive relations about the inboard body $B_{c(i)}$ are

$$\begin{cases} {}^p v_i^{c(i)} = {}^p v_{c(i)} - \mathbf{I}_{c(i)}^\times {}^p \omega_{c(i)} \\ {}^p \omega_i^{c(i)} = {}^p \omega_{c(i)} \\ \omega_i^{c(i)} = \omega_{c(i)} \\ \dot{v}_{it}^{c(i)} = \dot{v}_{c(i)t} - \mathbf{I}_{c(i)}^\times \dot{\omega}_{c(i)t} + \omega_{c(i)}^\times \omega_{c(i)}^\times \mathbf{I}_{c(i)} \\ \dot{\omega}_{it}^{c(i)} = \dot{\omega}_{c(i)t} \end{cases} \tag{12}$$

where $\mathbf{I}_{c(i)}$ is the vector from the origin of $F_i^{c(i)}$ to the one of F_i . The superscript “ $c(i)$ ” on the right side of the equal sign in Equation (12) denotes that the corresponding quantity is related to $F_i^{c(i)}$. The recursive relations about body B_i are

$$\begin{cases} {}^p v_i = \mathbf{A}(q_i) {}^p v_i^{c(i)} \\ {}^p \omega_i = \mathbf{A}(q_i) {}^p \omega_i^{c(i)} + \mathbf{\Gamma}_i \Delta_i \\ \omega_i = \mathbf{A}(q_i) \omega_i^{c(i)} + \mathbf{\Gamma}_i \dot{q}_i \\ \dot{v}_{it} = \mathbf{A}(q_i) \dot{v}_{it}^{c(i)} \\ \dot{\omega}_{it} = \mathbf{A}(q_i) \dot{\omega}_{it}^{c(i)} + \omega_i^\times \mathbf{\Gamma}_i \dot{q}_i \end{cases} \tag{13}$$

where $\Delta_i = \begin{bmatrix} 0 & \dots & 0 & \underbrace{1}_i & 0 & \dots & 0 \end{bmatrix} \in \mathbf{R}^{1 \times (6+n)}$. $\mathbf{A}(q_i)$ is the transformation matrix from frame $F_i^{c(i)}$ to frame F_i . According to Equations (12) and (13), the kinematics recursions between $B_i (i = 1, 2, \dots, n)$ and $B_{c(i)}$ excluding the platform B_0 can be obtained.

Denote the inboard body of the platform as $B_{c(0)}$. Suppose $B_{c(0)}$ is fixed on the inertial frame F_e , and B_0 connects with $B_{c(0)}$ by a virtual joint. Then the five kinematics quantities of the platform B_0 can be obtained according to the kinematics recursions between the platform and its inboard body in the following form

$$\begin{cases} {}^p v_0 = \begin{bmatrix} \mathbf{I}_3 & \mathbf{0}_{3 \times (3+n)} \end{bmatrix} \\ {}^p \omega_0 = \begin{bmatrix} \mathbf{0}_{3 \times 3} & \mathbf{I}_3 & \mathbf{0}_{3 \times n} \end{bmatrix} \\ \omega_0 = \omega_0 \\ \dot{v}_{0t} = \omega_0^\times v_0 \\ \dot{\omega}_{0t} = \omega_0^\times \omega_0 \end{cases} \tag{14}$$

The attitude kinematic equation of the platform can be written as

$$\omega_b = \mathbf{G}(\Theta_b) \dot{\Theta}_b \tag{15}$$

where $\Theta_b = [\phi \quad \theta \quad \psi]^T, \mathbf{G}(\Theta_b) = \begin{bmatrix} \cos \theta & 0 & -\cos \phi \sin \theta \\ 0 & 1 & \sin \phi \\ \sin \theta & 0 & \cos \phi \cos \theta \end{bmatrix}$.

4. Controller Design

4.1. Problem Statement

Denoting $\mathbf{V}_b = [v_b^T \quad \omega_b^T]^T, \mathbf{F}_b = [f_b^T \quad \tau_b^T]^T$, the dynamic equations in Equation (11) can be rewritten as

$$\begin{bmatrix} \mathbf{M}_b & \mathbf{M}_{bm} \\ \mathbf{M}_{bm}^T & \mathbf{M}_m \end{bmatrix} \begin{bmatrix} \dot{v}_b \\ \dot{q} \end{bmatrix} + \begin{bmatrix} \mathbf{F}_b^{lt} \\ \mathbf{F}_m^{lt} \end{bmatrix} = \begin{bmatrix} \mathbf{F}_b \\ -\mathbf{H} - \mathbf{B}\dot{h} \end{bmatrix} + \begin{bmatrix} 0 \\ \tau_d \end{bmatrix} \tag{16}$$

where $M_b \in R^{6 \times 6}$, $M_m \in R^{n \times n}$ and $M_{bm} \in R^{6 \times n}$ are the decomposition terms of the mass matrix M and their physical meanings are the inertia matrix of platform, the inertia matrix of manipulators and the coupling inertia matrix between the platform and manipulators, respectively. $F_b^{lt} \in R^6$ and $F_m^{lt} \in R^n$ are the decomposition terms of the nonlinear generalized inertia forces F^{lt} . According to Equation (16), the dynamic equations of manipulators can be obtained

$$(M_m - M_{bm}^T M_b^{-1} M_{bm}) \ddot{q} + (F_m^{lt} - M_{bm}^T M_b^{-1} F_b^{lt}) = -H - B\dot{h} - M_{bm}^T M_b^{-1} F_b + \tau_d \tag{17}$$

Let $M^* = M_m - M_{bm}^T M_b^{-1} M_{bm}$, $F^{lt*} = F_m^{lt} - M_{bm}^T M_b^{-1} F_b^{lt}$, then the equivalent dynamic equations of manipulators can be redescribed as follows

$$M^* \ddot{q} + F^{lt*} = -H - B\dot{h} - M_{bm}^T M_b^{-1} F_b + \tau_d \tag{18}$$

It is assumed that the space manipulator system described by Equation (18) has some known parts and some unknown parts considering parameter uncertainties and disturbance inputs. Therefore, M^* and F^{lt*} can be described by

$$M^* = M_0^* + \Delta M^* \tag{19}$$

$$F^{lt*} = F_0^{lt*} + \Delta F^{lt*} \tag{20}$$

where M_0^* and F_0^{lt*} are the known parts called nominal terms with the nominal parameters, ΔM^* and ΔF^{lt*} are the unknown parts with the inertia parameter uncertainties (the differences between the true parameters and the nominal parameters). In this research, we make the following assumption:

Assumption 1. M_0^* is invertible.

Let $q_d \in R^n$ represent the desired tracking trajectory that manipulators must follow and then the output tracking error can be defined as $e = q - q_d$. Thus the system error dynamic equations of manipulators can be described by in the following form

$$\ddot{e} = u_c - (M_0^*)^{-1} (H + F_0^{lt*}) - \ddot{q}_d + f_d \tag{21}$$

where $u_c \in R^n$ is the generalized control torque which is expressed as

$$u_c = -(M_0^*)^{-1} (B\dot{h} + M_{bm}^T M_b^{-1} F_b) \tag{22}$$

$f_d \in R^n$ is the combination of system parameter uncertainties and external disturbances of the space robot, which is defined as the lumped uncertainty, and it is expressed as

$$f_d = (M_0^*)^{-1} (\tau_d - \Delta M^* \ddot{q} - \Delta F^{lt*}) \tag{23}$$

According to Equation (23), the lumped uncertainty is both internal and external, as well as parametric and characteristic. According to Equation (23), the lumped uncertainty includes both internal modelling error and external interference error. Therefore, the lumped uncertainty is related on both time and system states, and its structure and parameters are normally unknown in practical engineering, which makes it a challenge for controller design of the space robot.

In the current methods, the unknown nonlinear equation f_d is usually assumed to be bounded with a prior knowledge [47]. A considerable drawback is that the requirement of prior knowledge of bounds of uncertainties is not viable in practice [30]. Therefore, a relatively complex control strategy is required for manipulators without a prior knowledge of the lumped uncertainty. Meanwhile, the dynamical coupling between the platform and manipulators still exists and the coupling effect of the platform on manipulators may affect

the control accuracy of the manipulator controller. Therefore, another control strategy is required for the platform to remain stationary.

By now the control objective in the present work becomes clear: design a trajectory tracking controller for manipulators with no prior knowledge of the lumped uncertainty and another pose controller for the platform to remain stationary relative to the inertial frame F_e . We propose to design an ANTSM trajectory tracking controller using RBFNN for manipulators first, then design a kinematic controller for the platform and finally accomplish the controller design for the whole system based on the inverse dynamics method. The block diagram of the whole closed-loop control system is depicted in Figure 2.

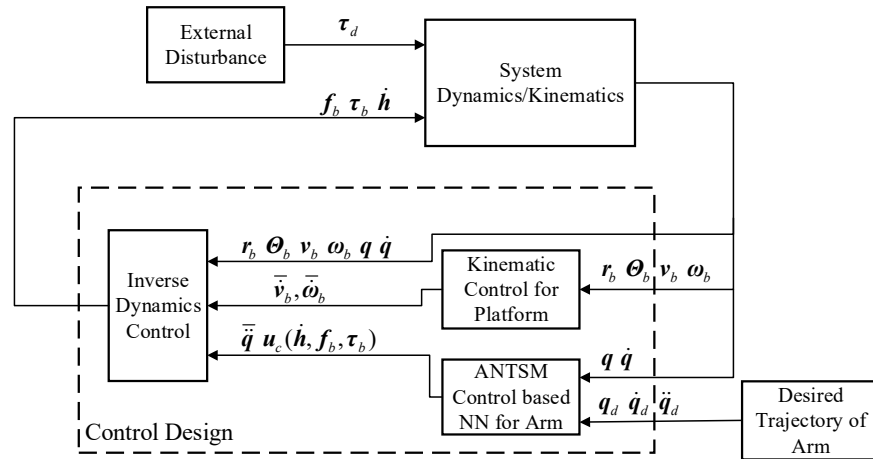


Figure 2. Block diagram of the closed-loop control system.

4.2. ANTSM Controller for Manipulators

In this section, we first use the RBFNN to approximate the nonlinear equation f_d so as to realize the compensation of the uncertainty in the control law. We then define a nonsingular terminal sliding surface and finally design the adaptive control law to accomplish the controller design for manipulators. The structure of the ANTSM control using RBFNN is shown in Figure 3.

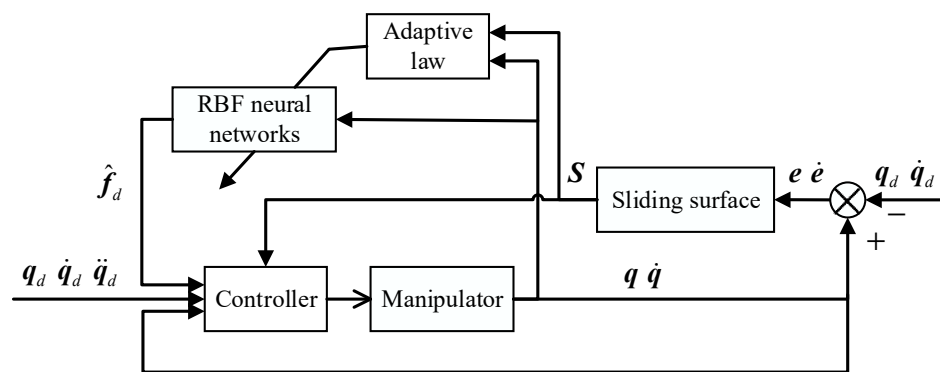


Figure 3. The structure of the ANTSM control using RBFNN.

4.2.1. RBF Neural Network

An RBF network is a kind of local approximation neural network. A new RBFNN is proposed to adaptively approximate the lumped uncertainty f_d , as shown in Figure 4. The estimate of the lumped uncertainty using the proposed RBFNN is defined as \hat{f}_d , and it can be designed as follows:

$$\hat{f}_d = \hat{W}^T \Phi(x) \tag{24}$$

where $x = [q^T \ \dot{q}^T]^T \in \mathbb{R}^{2n}$ is the input state vector, m is the number of neurons, and $\hat{W} \in \mathbb{R}^{m \times n}$ is the estimate of the ideal approximation weight which is described by

$$\hat{W} = \begin{bmatrix} \hat{w}_{11} & \hat{w}_{12} & \cdots & \hat{w}_{1n} \\ \hat{w}_{21} & \hat{w}_{22} & \cdots & \hat{w}_{2n} \\ \vdots & \vdots & \cdots & \vdots \\ \hat{w}_{m1} & \hat{w}_{m2} & \cdots & \hat{w}_{mn} \end{bmatrix} \quad (25)$$

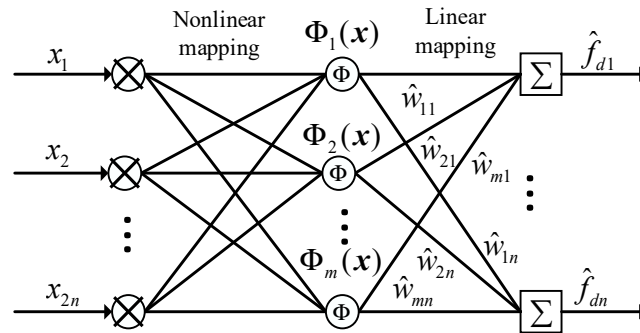


Figure 4. The structure of RBFNN.

$\Phi(x) = [\Phi_1(x) \ \Phi_2(x) \ \cdots \ \Phi_m(x)]^T \in \mathbb{R}^m$ is the vector of Gaussian type of functions whose elements are defined as

$$\Phi_i(x) = \exp\left(-\frac{\|x - c_i\|^2}{\sigma_i^2}\right) \quad (i = 1, 2, \dots, m) \quad (26)$$

where the vector $c_i \in \mathbb{R}^{2n} (i = 1, 2, \dots, m)$ is the center of the i -th Gaussian function, $\sigma_i \in \mathbb{R}$ is a width parameter around the center point. For further analysis, we make the following assumption:

Assumption 2. Let ε represent the approximation error of the RBFNN defined as $\varepsilon = f_d - \hat{f}_d$. Given an arbitrary small positive constant $\varepsilon_N > 0$, the norm of the approximation error and the constant satisfy the following relationship:

$$\|\varepsilon\| \leq \varepsilon_N \quad (27)$$

4.2.2. Sliding Surface

A nonsingular terminal sliding surface is a nonlinear function of the tracking error defined in Ref. [48]:

$$S = e + \frac{1}{\beta} \dot{e}^{p/q} \quad (28)$$

where β is a positive parameter to be designed, p and q are positive odd numbers with $1 < p/q < 2$. When the sliding mode of the system reaches the sliding surface with $s_i = e_i + \frac{1}{\beta} \dot{e}_i^{p/q} = 0$ where variables s_i and e_i are elements of the sliding surface vector S and the tracking error vector e , it is obvious that the trajectory tracking error can approach zero in finite time t_f which is derived as:

$$t_f = \frac{e_{i0}^{1-q/p}}{(1 - q/p)\beta^{-q/p}} \quad (29)$$

where e_{i0} is the initial value of the tracking error element e_i .

4.2.3. Control Law Design

After constructing the nonsingular terminal sliding surface S , the next phase for the controller is to design the adaptive control law so that the reaching condition $S^T \dot{S} < 0$ is satisfied. Based on the equivalent control concept, the adaptive nonsingular terminal sliding mode control based on RBFNN can be implemented:

$$u_c = -\frac{\beta q}{p} \text{diag}(\dot{e}^{3-p/q}) K S - \hat{f}_d + u_{eq} + u_N \tag{30}$$

where $K \in \mathbb{R}^{n \times n}$ is a positive definite symmetric matrix and u_{eq} is the equivalent control for the system dynamic Equation (21), determined by

$$u_{eq} = (M_0^*)^{-1} (H + F_0^{It*}) + \ddot{q}_d - \frac{\beta q}{p} \dot{e}^{2-p/q} \tag{31}$$

The term u_N is designed to overcome influence of system instability caused by the approximation error of the RBFNN ε , given by

$$u_N = -\text{sign}(\text{diag}(\dot{e}^{p/q-1}) S) \varepsilon_N \tag{32}$$

where “ $\text{sign}(\cdot)$ ” indicates the symbolic function, defined as

$$\text{sign}(a) = \begin{cases} 1 & a > 0 \\ 0 & a = 0 \\ -1 & a < 0 \end{cases} \tag{33}$$

The term \hat{f}_d derived as Equation (24) is the estimate vector of the lumped uncertainty. To make \hat{f}_d approximate the lumped uncertainty f_d adaptively, a new weight update law is proposed

$$\dot{W} = \alpha \Phi(x) \left(\frac{p}{\beta q} \text{diag}(\dot{e}^{p/q-1}) S \right)^T \tag{34}$$

where α is a positive parameter to be designed. The exponents of \dot{e} in Equations (30)–(34) are all greater than 0 due to $1 < p/q < 2$, therefore the proposed adaptive control law based on RBFNN in Equation (30) is nonsingular.

4.3. Kinematic Controller for Platform

In this section, we design a kinematic controller for the platform to keep the position and attitude of the platform relative to the inertial frame F_e unchanged, thereby reducing the impact of the platform coupling on the control accuracy of manipulators.

4.3.1. Attitude Control

Differentiating Equation (15) with respect to time, we have

$$\dot{\omega}_b = G \ddot{\Theta}_b + \dot{G} \dot{\Theta}_b \tag{35}$$

Since G is always reversible, we can get $\dot{\Theta}_b = G^{-1} \omega_b$ according to Equation (15) Then, substituting $\dot{\Theta}_b = G^{-1} \omega_b$ into Equation (35) the attitude kinematic relation for the platform in Equation (35) can be rewritten as

$$\dot{\omega}_b = G \ddot{\Theta}_b + \dot{G} G^{-1} \omega_b \tag{36}$$

Finally, we design an attitude control law based on PD control strategy as follows

$$\dot{\omega}_b = G(-K_{d1} G^{-1} \omega_b - K_{p1} \Theta_b) + \dot{G} G^{-1} \omega_b \tag{37}$$

where $\dot{\omega}_b \in \mathbb{R}^{3 \times 1}$ is the command angular acceleration for the platform, and $K_{d1} \in \mathbb{R}^{3 \times 3}$ and $K_{p1} \in \mathbb{R}^{3 \times 3}$ are the control parameter matrices of the PD attitude control law.

4.3.2. Position Control

It is easy to obtain the relationship of the position r_b and the linear velocity v_b of the platform according to their definitions

$$v_b = A(\Theta_b)^T \dot{r}_b \tag{38}$$

Differentiating Equation (38) with respect to time, we have

$$\dot{v}_b = A(\Theta_b)^T \ddot{r}_b - \omega_b^\times v_b \tag{39}$$

Then we can design a position control law based on the same control strategy with the previous section

$$\dot{v}_b = A(\Theta_b)^T (-K_{d2} \dot{r}_b - K_{p2} r_b) - \omega_b^\times v_b \tag{40}$$

where $\dot{v}_b \in \mathbb{R}^{3 \times 1}$ is the command linear acceleration for the platform, $K_{d2} \in \mathbb{R}^{3 \times 3}$ and $K_{p2} \in \mathbb{R}^{3 \times 3}$ are the control parameter matrices of the PD position control law.

4.4. Inverse Dynamics Controller for System

In this section, we accomplish the controller design for the whole system based on the inverse dynamics method. The equivalent dynamic equations of manipulators in Equation (21) can be rewritten as

$$\ddot{q} = u_c - (M_0^*)^{-1} (H + F_0^{It*}) + f_d \tag{41}$$

Substituting the generalized control torque u_c designed in Equation (30) and the estimate of the lumped uncertainty \hat{f}_d designed in Equation (24) into Equation (41), we can obtain the command joint accelerations \ddot{q} as follows

$$\ddot{q} = u_c - (M_0^*)^{-1} (H + F_0^{It*}) + \hat{f}_d \tag{42}$$

According to the dynamic equations in Equation (16), we can obtain the following equation

$$M_b \begin{bmatrix} \dot{v}_b^T & \dot{\omega}_b^T \end{bmatrix}^T + M_{bm} \ddot{q} + F_b^{It} = F_b \tag{43}$$

Substituting the command accelerations \dot{v}_b in Equation (40), $\dot{\omega}_b$ in Equation (37) and \ddot{q} in Equation (42), then the active control forces and torques for the platform in the designed inverse dynamics controller can be obtained as

$$F_b = M_b \begin{bmatrix} -T & -T \end{bmatrix}^T + M_{bm} \ddot{q} + F_b^{It} \tag{44}$$

Substituting the generalized control torque u_c designed in Equation (30) and the active control forces and torques for the platform F_b in Equation (44) into Equation (22), then the time derivative of angular momentum of CMGs can be calculated by

$$\dot{h} = -B^{-1} (M_0^* u_c + M_{bm}^T M_b^{-1} F_b) \tag{45}$$

4.5. Stability Analysis

In this section, we analyze the stability of the designed controllers. Since the PD control strategy and inverse dynamics method have been quite mature, their stability is easy to prove. Therefore, we only analyze the stability of the ANTSM controller using RBFNN for manipulators.

Firstly, we substitute the proposed controller in Equation (30) into Equation (21), and we can get the closed-loop error equation as follows

$$\ddot{e} = -\frac{\beta q}{p} \dot{e}^{2-p/q} - \frac{\beta q}{p} \text{diag}(\dot{e}^{3-p/q}) \mathbf{KS} - \hat{\mathbf{f}} + \mathbf{f}_d - \text{sign}(\text{diag} \dot{e}^{p/q-1} \mathbf{S}) \varepsilon_N \quad (46)$$

Let $\tilde{\mathbf{W}}$ represent the estimate error of the weight matrix for neural network defined as

$$\tilde{\mathbf{W}} = \mathbf{W} - \hat{\mathbf{W}} \in \mathbf{R}^{m \times n} \quad (47)$$

Differentiating the sliding surface \mathbf{S} with respect to time and using Equation (24) and Equation (46), we can obtain that

$$\begin{aligned} \dot{\mathbf{S}} &= \dot{e} + \frac{p}{\beta q} \text{diag}(\dot{e}^{p/q-1}) \left(-\frac{\beta q}{p} \dot{e}^{2-p/q} - \frac{\beta q}{p} \text{diag}(\dot{e}^{3-p/q}) \mathbf{KS} - \hat{\mathbf{f}} + \mathbf{f}_d - \text{sign}(\text{diag} \dot{e}^{p/q-1} \mathbf{S}) \varepsilon_N \right) \\ &= \frac{p}{\beta q} \text{diag}(\dot{e}^{p/q-1}) \left(-\frac{\beta q}{p} \text{diag}(\dot{e}^{3-p/q}) \mathbf{KS} - \hat{\mathbf{f}} + \mathbf{f}_d - \text{sign}(\text{diag} \dot{e}^{p/q-1} \mathbf{S}) \varepsilon_N \right) \\ &= -\text{diag}(\dot{e}^2) \mathbf{KS} + \frac{p}{\beta q} \text{diag}(\dot{e}^{p/q-1}) \left(-\hat{\mathbf{f}} + \mathbf{f}_d - \text{sign}(\text{diag} \dot{e}^{p/q-1} \mathbf{S}) \varepsilon_N \right) \\ &= -\text{diag}(\dot{e}^2) \mathbf{KS} + \frac{p}{\beta q} \text{diag}(\dot{e}^{p/q-1}) \left(-\tilde{\mathbf{W}}^T \Phi(\mathbf{x}) + \mathbf{W}^T \Phi(\mathbf{x}) + \varepsilon - \text{sign}(\text{diag} \dot{e}^{p/q-1} \mathbf{S}) \varepsilon_N \right) \\ &= -\text{diag}(\dot{e}^2) \mathbf{KS} + \frac{p}{\beta q} \text{diag}(\dot{e}^{p/q-1}) \left(\tilde{\mathbf{W}}^T \Phi(\mathbf{x}) + \varepsilon - \text{sign}(\text{diag} \dot{e}^{p/q-1} \mathbf{S}) \varepsilon_N \right) \end{aligned} \quad (48)$$

The performance of the control law can be stated by the following theorem.

Theorem 1. Given the error dynamics in Equation (21) for manipulators with Assumptions 1 and 2, if the nonsingular terminal sliding manifold is chosen as Equation (28) the controller is chosen as Equation (30) with \mathbf{u}_{eq} given by Equation (31), \mathbf{u}_N given by Equation (32) and $\hat{\mathbf{f}}_d$ given by Equation (24) with the weight update law given by Equation (34), then the closed-loop system of manipulators is asymptotically stable.

Proof of Theorem 1. Select the following Lyapunov function. \square

$$V = \frac{1}{2} \mathbf{S}^T \mathbf{S} + \frac{1}{2} \text{tr}(\alpha^{-1} \tilde{\mathbf{W}}^T \tilde{\mathbf{W}}) \quad (49)$$

where $\text{tr}(\cdot)$ represents the trace operator and $\dot{\tilde{\mathbf{W}}} = -\dot{\hat{\mathbf{W}}}$.

Differentiating V with respect to time and using Equation (34) and Equation (48), we can obtain that

$$\begin{aligned} \dot{V} &= \mathbf{S}^T \dot{\mathbf{S}} + \text{tr}(\alpha^{-1} \tilde{\mathbf{W}}^T \dot{\tilde{\mathbf{W}}}) \\ &= -\mathbf{S}^T \text{diag}(\dot{e}^2) \mathbf{KS} + \mathbf{S}^T \frac{p}{\beta q} \text{diag}(\dot{e}^{p/q-1}) \left(\tilde{\mathbf{W}}^T \Phi(\mathbf{x}) + \varepsilon - \text{sign}(\text{diag} \dot{e}^{p/q-1} \mathbf{S}) \varepsilon_N \right) \\ &\quad - \text{tr}(\tilde{\mathbf{W}}^T \Phi(\mathbf{x}) \left(\frac{p}{\beta q} \text{diag}(\dot{e}^{p/q-1}) \mathbf{S} \right)^T) \\ &= -\mathbf{S}^T \mathbf{K}_e \mathbf{S} + \mathbf{S}^T \frac{p}{\beta q} \text{diag}(\dot{e}^{p/q-1}) \varepsilon - \mathbf{S}^T \frac{p}{\beta q} \text{diag}(\dot{e}^{p/q-1}) \text{sign}(\text{diag} \dot{e}^{p/q-1} \mathbf{S}) \varepsilon_N \\ &\quad + \mathbf{S}^T \frac{p}{\beta q} \text{diag}(\dot{e}^{p/q-1}) \tilde{\mathbf{W}}^T \Phi(\mathbf{x}) - \text{tr}(\tilde{\mathbf{W}}^T \Phi(\mathbf{x}) \left(\frac{p}{\beta q} \text{diag}(\dot{e}^{p/q-1}) \mathbf{S} \right)^T) \end{aligned} \quad (50)$$

Then using Equation (27), we can obtain that

$$\begin{aligned} \dot{V} &\leq -\mathbf{S}^T \mathbf{K}_e \mathbf{S} + \frac{p}{\beta q} \|\mathbf{S}^T \text{diag}(\dot{e}^{p/q-1})\| (\|\boldsymbol{\varepsilon}\| - \varepsilon_N) \\ &\quad + \mathbf{S}^T \frac{p}{\beta q} \text{diag}(\dot{e}^{p/q-1}) \tilde{\mathbf{W}}^T \boldsymbol{\Phi}(\mathbf{x}) - \text{tr}(\tilde{\mathbf{W}}^T \boldsymbol{\Phi}(\mathbf{x}) (\frac{p}{\beta q} \text{diag}(\dot{e}^{p/q-1}) \mathbf{S})^T) \\ &\leq -\mathbf{S}^T \mathbf{K}_e \mathbf{S} + \mathbf{S}^T \frac{p}{\beta q} \text{diag}(\dot{e}^{p/q-1}) \tilde{\mathbf{W}}^T \boldsymbol{\Phi}(\mathbf{x}) - (\frac{p}{\beta q} \text{diag}(\dot{e}^{p/q-1}) \mathbf{S})^T \tilde{\mathbf{W}}^T \boldsymbol{\Phi}(\mathbf{x}) \quad (51) \\ &\leq -\mathbf{S}^T \mathbf{K}_e \mathbf{S} + \mathbf{S}^T \frac{p}{\beta q} \text{diag}(\dot{e}^{p/q-1}) \tilde{\mathbf{W}}^T \boldsymbol{\Phi}(\mathbf{x}) - \mathbf{S}^T \frac{p}{\beta q} \text{diag}(\dot{e}^{p/q-1}) \tilde{\mathbf{W}}^T \boldsymbol{\Phi}(\mathbf{x}) \\ &\leq -\mathbf{S}^T \mathbf{K}_e \mathbf{S} \end{aligned}$$

where $\mathbf{K}_e = \text{diag}(\dot{e}^2) \mathbf{K}$ is a positive definite symmetric matrix, then $\dot{V} \leq -\mathbf{S}^T \mathbf{K}_e \mathbf{S} \leq 0$ is satisfied, consequently the tracking error can asymptotically converge to zero as requested by the Lyapunov method.

For practical implementations, the proposed controller should be smoothed to avoid chattering problems. To address the problem, a smoothed control \mathbf{u}_N in Equation (32) is redesigned as follows

$$\mathbf{u}_N = -\text{sat}(\text{diag}\dot{e}^{p/q-1} \mathbf{S}) \boldsymbol{\varepsilon}_N \quad (52)$$

where $\text{sat}(\cdot)$ represents the saturation function, defined as

$$\text{sat}(\text{diag}\dot{e}^{p/q-1} \mathbf{S}) = \begin{cases} \text{sign}(\text{diag}\dot{e}^{p/q-1} \mathbf{S}) & \|\text{diag}\dot{e}^{p/q-1} \mathbf{S}\| > \delta \\ \frac{\text{diag}\dot{e}^{p/q-1} \mathbf{S}}{\delta} & \|\text{diag}\dot{e}^{p/q-1} \mathbf{S}\| \leq \delta \end{cases} \quad (53)$$

where δ is a positive parameter to be designed.

Theorem 2. Given the error dynamics in Equation (21) for manipulators with Assumptions 1 and 2, if the nonsingular terminal sliding manifold is chosen as Equation (28), the controller is chosen as Equation (30) with \mathbf{u}_{eq} given by Equation (31), \mathbf{u}_N given by Equation (52) and $\hat{\mathbf{f}}_d$ given by Equation (24), with the weight update law given by Equation (34), then the closed-loop system of manipulators is uniformly ultimately bounded.

Proof of Theorem 2. Substituting the proposed controller in Equation (52) into Equation (21), we can get the closed-loop error equation as follows. \square

$$\ddot{e} = -\frac{\beta q}{p} \dot{e}^{2-p/q} - \frac{\beta q}{p} \text{diag}(\dot{e}^{3-p/q}) \mathbf{K} \mathbf{S} - \hat{\mathbf{f}} + \mathbf{f}_d - \text{sat}(\text{diag}\dot{e}^{p/q-1} \mathbf{S}) \boldsymbol{\varepsilon}_N \quad (54)$$

Then the derivative of the sliding manifold becomes

$$\dot{\mathbf{S}} = -\text{diag}(\dot{e}^2) \mathbf{K} \mathbf{S} + \frac{p}{\beta q} \text{diag}(\dot{e}^{p/q-1}) (\tilde{\mathbf{W}}^T \boldsymbol{\Phi}(\mathbf{x}) + \boldsymbol{\varepsilon} - \text{sat}(\text{diag}\dot{e}^{p/q-1} \mathbf{S}) \boldsymbol{\varepsilon}_N) \quad (55)$$

Select the Lyapunov function as Equation (49). Differentiating V with respect to time, the time derivative of V can be rewritten as

$$\begin{aligned} \dot{V} &= -\mathbf{S}^T \mathbf{K}_e \mathbf{S} + \mathbf{S}^T \frac{p}{\beta q} \text{diag}(\dot{e}^{p/q-1}) \boldsymbol{\varepsilon} - \mathbf{S}^T \frac{p}{\beta q} \text{diag}(\dot{e}^{p/q-1}) \text{sat}(\text{diag}\dot{e}^{p/q-1} \mathbf{S}) \boldsymbol{\varepsilon}_N \\ &\quad + \mathbf{S}^T \frac{p}{\beta q} \text{diag}(\dot{e}^{p/q-1}) \tilde{\mathbf{W}}^T \boldsymbol{\Phi}(\mathbf{x}) - \text{tr}(\tilde{\mathbf{W}}^T \boldsymbol{\Phi}(\mathbf{x}) (\frac{p}{\beta q} \text{diag}(\dot{e}^{p/q-1}) \mathbf{S})^T) \\ &\leq -\mathbf{S}^T \mathbf{K}_e \mathbf{S} + \frac{p}{\beta q} \|\mathbf{S}^T \text{diag}(\dot{e}^{p/q-1})\| \|\boldsymbol{\varepsilon}\| - \frac{p}{\beta q} \mathbf{S}^T \text{diag}(\dot{e}^{p/q-1}) \text{sat}(\text{diag}\dot{e}^{p/q-1} \mathbf{S}) \boldsymbol{\varepsilon}_N \quad (56) \\ &\quad + \mathbf{S}^T \frac{p}{\beta q} \text{diag}(\dot{e}^{p/q-1}) \tilde{\mathbf{W}}^T \boldsymbol{\Phi}(\mathbf{x}) - (\frac{p}{\beta q} \text{diag}(\dot{e}^{p/q-1}) \mathbf{S})^T \tilde{\mathbf{W}}^T \boldsymbol{\Phi}(\mathbf{x}) \\ &\leq -\mathbf{S}^T \mathbf{K}_e \mathbf{S} + \frac{p}{\beta q} \|\mathbf{S}^T \text{diag}(\dot{e}^{p/q-1})\| \|\boldsymbol{\varepsilon}\| - \frac{p}{\beta q} \mathbf{S}^T \text{diag}(\dot{e}^{p/q-1}) \text{sat}(\text{diag}\dot{e}^{p/q-1} \mathbf{S}) \boldsymbol{\varepsilon}_N \end{aligned}$$

If $\|\text{diag}\dot{e}^{p/q-1} \mathbf{S}\| > \delta$, then $\text{sat}(\text{diag}\dot{e}^{p/q-1} \mathbf{S}) = \text{sign}(\text{diag}\dot{e}^{p/q-1} \mathbf{S})$ and it can be proved that

$$\dot{V} \leq -\mathbf{S}^T \mathbf{K}_e \mathbf{S} \leq 0 \quad (57)$$

If $\|diag\dot{e}^{p/q-1}\mathbf{S}\| \leq \delta$, then $sat(diag\dot{e}^{p/q-1}\mathbf{S}) = \frac{diag\dot{e}^{p/q-1}\mathbf{S}}{\delta}$ and it can be proved that

$$\begin{aligned} \dot{V} &\leq -\mathbf{S}^T\mathbf{K}_e\mathbf{S} + \frac{p}{\beta q}\|\mathbf{S}^Tdiag(\dot{e}^{p/q-1})\|\|\boldsymbol{\varepsilon}\| - \frac{p}{\beta q}\mathbf{S}^Tdiag(\dot{e}^{p/q-1})sat(diag\dot{e}^{p/q-1}\mathbf{S})\boldsymbol{\varepsilon}_N \\ &\leq -\mathbf{S}^T\mathbf{K}_e\mathbf{S} + \frac{p}{\beta q}\|\mathbf{S}^Tdiag(\dot{e}^{p/q-1})\|\boldsymbol{\varepsilon}_N - \frac{p}{\beta q}\mathbf{S}^Tdiag(\dot{e}^{p/q-1})sat(diag\dot{e}^{p/q-1}\mathbf{S})\boldsymbol{\varepsilon}_N \\ &\leq -\mathbf{S}^T\mathbf{K}_e\mathbf{S} + \frac{p}{\beta q}(\|\mathbf{S}^Tdiag(\dot{e}^{p/q-1})\| - \mathbf{S}^Tdiag(\dot{e}^{p/q-1})sat(diag\dot{e}^{p/q-1}\mathbf{S}))\boldsymbol{\varepsilon}_N \quad (58) \\ &\leq -\mathbf{S}^T\mathbf{K}_e\mathbf{S} + \frac{p}{\beta q}\|\mathbf{S}^Tdiag(\dot{e}^{p/q-1})\|\boldsymbol{\varepsilon}_N \\ &\leq -\mathbf{S}^T\mathbf{K}_e\mathbf{S} + \frac{p}{\beta q}\delta\boldsymbol{\varepsilon}_N \end{aligned}$$

where $\frac{p}{\beta q}\delta\boldsymbol{\varepsilon}_N$ is a positive constant. With Equations (57) and (58), the closed-loop system of manipulators is uniformly ultimately bounded [49].

5. Numerical Simulation

5.1. Simulation Parameters

To demonstrate the effectiveness of the proposed controllers, the closed-loop SRS with a platform and three single-degree-of-freedom manipulator arms is simulated in this section. The simulation task is to enable the robotic manipulators to track the specified trajectory accurately in joint space and keep the platform stationary relative to the inertial frame.

The inertia parameters of the system are listed in Table 1 and the Denavit-Hartenberg parameters of the manipulator are shown in Table 2.

The desired trajectories of the joints are given by

$$\mathbf{q}_d = \begin{bmatrix} \pi/2 \\ 0.1e^{-t} - 0.025e^{-4t} - 0.075 \\ -0.14e^{-t} + 0.035e^{-4t} + 0.305 \end{bmatrix} \text{ (rad)} \quad (59)$$

Table 1. System inertia and installation parameters.

Body Number	Mass (kg)		First Moment (kg·m)	Inertia Matrix (kg·m ²)	
	True	Nominal		True	Nominal
B ₀		1600	$[0 \ 0 \ 0]^T$	$diag(2000, 2000, 900)$	
B ₁	1.37	1.2	$[0 \ 0 \ 0.0685]^T$	$diag(5.1, 5.1, 1.1) \times 10^{-3}$	$diag(4.7, 4.7, 1.1) \times 10^{-3}$
B ₂	24.72	22	$[19.1 \ 0 \ 4]^T$	$\begin{bmatrix} 0.69 & 0 & -3.25 \\ 0 & 23.03 & 0 \\ -3.25 & 0 & 22.37 \end{bmatrix}$	$\begin{bmatrix} 0.62 & 0 & -2.91 \\ 0 & 21.33 & 0 \\ -2.91 & 0 & 20.75 \end{bmatrix}$
B ₃	24.86	22	$[19.1 \ 0 \ -4.7]^T$	$\begin{bmatrix} 0.93 & 0 & 3.78 \\ 0 & 23.28 & 0 \\ 3.78 & 0 & 22.36 \end{bmatrix}$	$\begin{bmatrix} 0.83 & 0 & 3.37 \\ 0 & 21.49 & 0 \\ 3.37 & 0 & 20.67 \end{bmatrix}$

Table 2. Denavit-Hartenberg parameters of the manipulator.

Body Number	a _i (m)	α _i (rad)	d _i (m)	θ _i (rad)
B ₁	0	0.5π	0.1	q ₁
B ₂	1.825	0	0.54	q ₂
B ₃	1.8825	0	0	q ₃

External interference is unknown in the real environment. However, the disturbance joint torques in the simulation are chosen as

$$\boldsymbol{\tau}_d = \begin{bmatrix} -\tanh(50\dot{q}_1) - 1.5\dot{q}_1 + 2 \\ -\tanh(50\dot{q}_2) - \dot{q}_2 + 2 \\ -\tanh(50\dot{q}_3) - 0.5\dot{q}_3 + 2 \end{bmatrix} \text{ (N} \cdot \text{m)} \quad (60)$$

where “tanh(·)” indicates the hyperbolic tangent function. Select simulation initial values are listed in Table 3, and the initial and desired configurations of the system are shown in Figure 5.

Table 3. Simulation initial values.

Parameter	Value
Initial positions of the platform (m)	$[0 \ 0 \ 0]^T$
Initial rotation angles of the platform (rad)	$[0 \ 0 \ 0]^T$
Initial linear velocities of the platform (m/s)	$[0 \ 0 \ 0]^T$
Initial angular velocities of the platform (rad/s)	$[0 \ 0 \ 0]^T$
Initial joint angles (rad)	$[\pi/12 \ \pi/6 \ \pi/2]^T$
Initial joint speeds (rad/s)	$[0 \ 0 \ 0]^T$
Initial angular momentums (Nms)	$[0 \ 0 \ 0]^T$

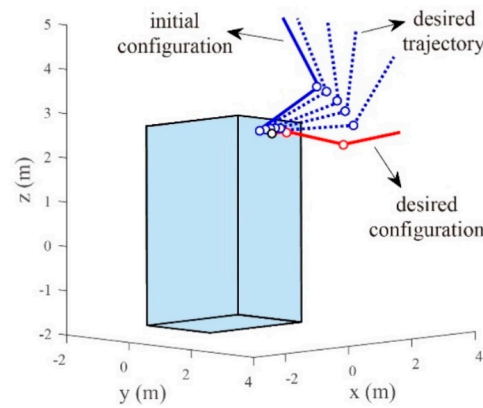


Figure 5. System initial and desired configurations.

The controller parameters are listed in Table 4.

Table 4. Controller parameters of the system.

Parameter	Value
The proportional gain K_{p1}	$diag[4.5 \ 4.5 \ 4.5]$
The derivative gain K_{d1}	$diag[5 \ 5 \ 5]$
The proportional gain K_{p2}	$diag[3 \ 3 \ 3]$
The derivative gain K_{d2}	$diag[3.5 \ 3.5 \ 3.5]$
The constant β	0.05
The odd number p	5
The odd number q	3
The constant δ	0.1
Upper bound of the estimate error ϵ_N	0.1
The constant α	0.4
Number of neurons m	10
Initial of weight matrix W_0	$zeros(10, 3)$
The gain matrix K	$diag[0.3 \ 0.25 \ 0.1]$

5.2. Simulation Results

5.2.1. Demonstration of Algorithm Effectiveness

The joint angle q and the angle tracking error $e = q - q_d$ are shown in Figure 6, and the joint angular velocity \dot{q} and the velocity tracking error $\dot{e} = \dot{q} - \dot{q}_d$ are illustrated in Figure 7. Figures 6 and 7 indicate that the robot manipulator system can track the desired trajectory

accurately even though the upper bounds of the system uncertainties are unknown, which can also be shown by Figure 8, where the terminal sliding variable S is presented.

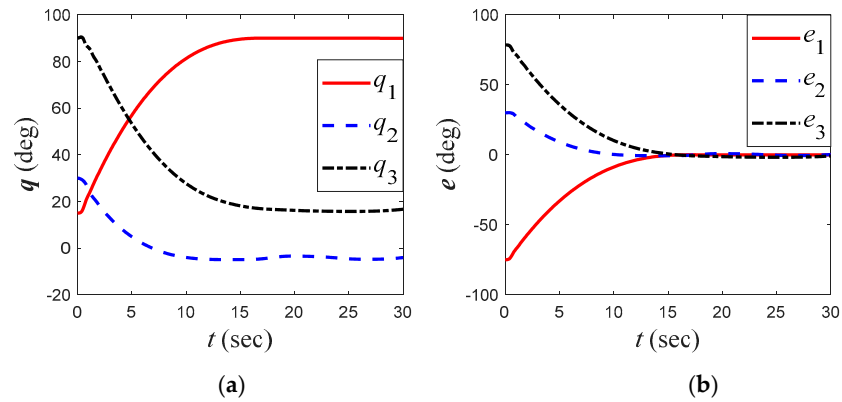


Figure 6. (a) Joint angles; (b) Joint angle tracking errors.

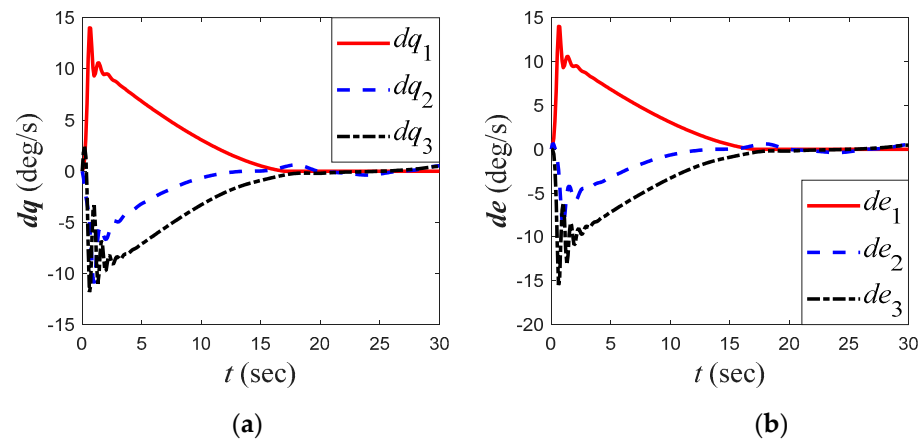


Figure 7. (a) Joint angular velocities; (b) Joint angular velocity tracking errors.

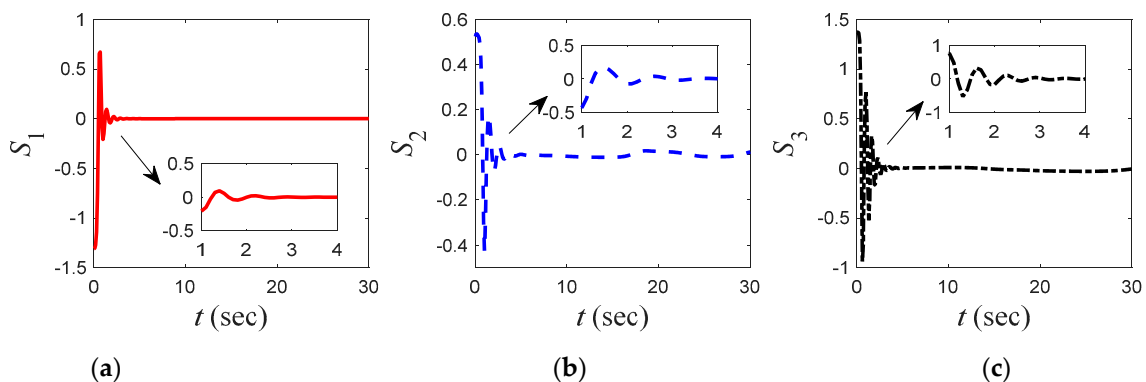


Figure 8. (a) The first value of the sliding manifold; (b) The second value of the sliding manifold; (c) The third value of the sliding manifold.

Observing Figure 9, we can see that the approximate errors $\varepsilon = f_d - \hat{f}_d$ using RBFNN converge to zero rapidly. It can also present that the output vector of the proposed network can adaptively approximate the lumped uncertainty f_d consisting of system parameter uncertainties and external disturbances. Comparing Figures 8 and 9, the initial fluctuation of the estimation error is roughly the same as that of the sliding surface, which is caused

by the compensation of the controller of the neural network estimation. The fluctuation frequency is within the tolerable fluctuation range of the space robot.

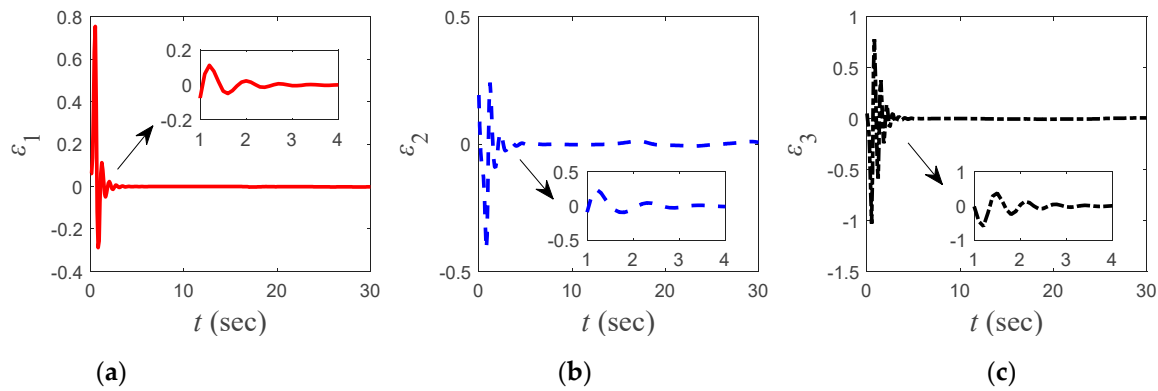


Figure 9. (a) The first value of the approximate errors of the lumped uncertainty; (b) The second value of the approximate errors of the lumped uncertainty; (c) The third value of the approximate errors of the lumped uncertainty.

To verify the estimation performance of the RBFNN, a cost function is chosen as

$$J = \frac{1}{n} \|\epsilon\| = \frac{1}{n} \|f_d - \hat{f}_d\| = \frac{1}{n} \sqrt{\sum_{i=1}^n \epsilon_i^2}$$

As shown in Figure 10, the cost function can converge to zero in a short time, which can also present that the proposed RBFNN can adaptively approximate the lumped uncertainty.

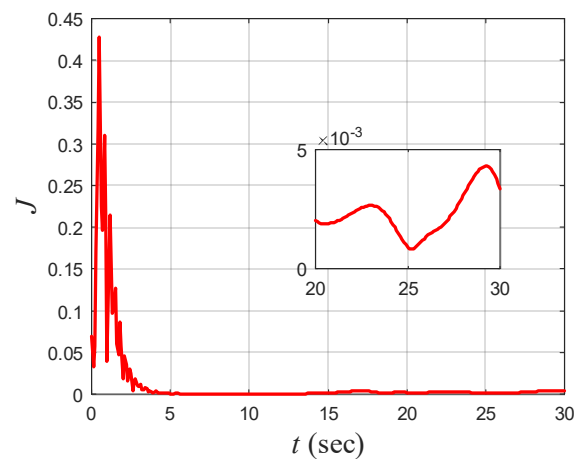


Figure 10. The cost function.

To investigate whether the platform is stationary during the control, the position and attitude of the platform are presented in Figure 11. Observing Figure 11 we can see the platform remains stationary relative to the inertial frame precisely with the position control accuracy reaching 0.5×10^{-3} m and the attitude pointing accuracy reaching 0.01° . Figure 12 shows the linear and angular velocities of the platform, respectively, with the attitude stability reaching $5 \times 10^{-3} \text{ }^\circ/\text{s}$.

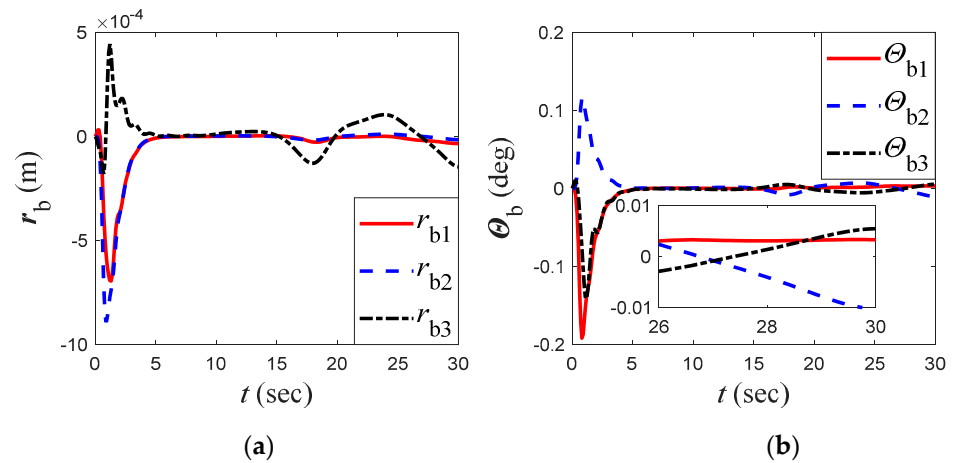


Figure 11. (a) Position of the platform; (b) attitude of the platform.

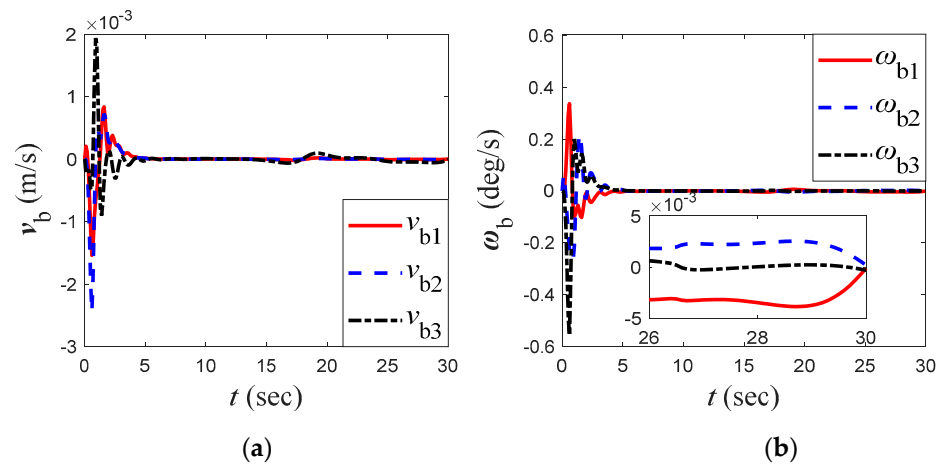


Figure 12. (a) Linear velocities of the platform; (b) angular velocities of the platform.

Figure 13 presents the control torque τ_m acting on the manipulator and the time derivatives of the angular momentums, i.e., \dot{h} , of the CMGs, which are all in the reasonable range of values. Since the manipulators can track the desired trajectory in a short time with a fast estimation speed and a fast convergence speed, the angular momentum saturation of the CMGs would not occur basically, as long as the initial angular momentum is not too large.

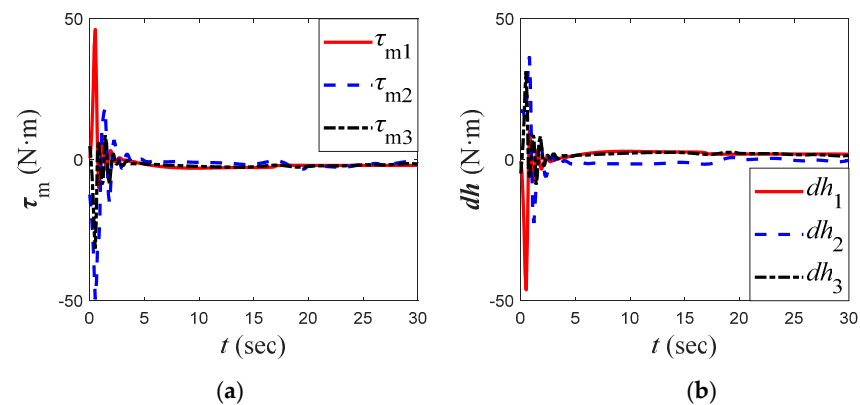


Figure 13. (a) Control torque of the manipulator; (b) The derivative of angular momentums of the CMGs.

The control force f_b and control torque τ_b acting on the platform are shown in Figure 14. The reason for the large magnitudes of the control torque in the initial stage of simulation is the large initial joint errors of the manipulators. The inverse dynamics control law (44) produces larger control torques to suppress the initial errors, resulting in preferable control accuracy.

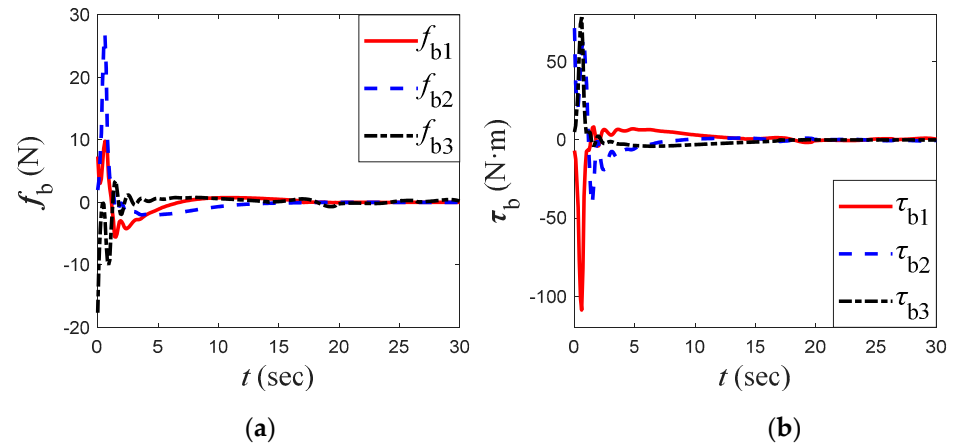


Figure 14. (a) Control forces of the platform; (b) Torques of the platform.

5.2.2. Comparison with Different Control Laws

In order to demonstrate the effectiveness of the RBFNN, we adopt the same ANTSM control law (30) without the estimate of the lumped uncertainty for comparison, that is $\hat{f}_d = 0_{3 \times 1}$. Comparisons of angle tracking errors and sliding manifolds under the ANTSM control law (30) with or without RBFNN are illustrated in Figures 15 and 16, respectively. It is obvious that both the angle errors and the sliding manifolds without NN are much larger than those with NN, which implies the significant role of NN in improving system control accuracy.

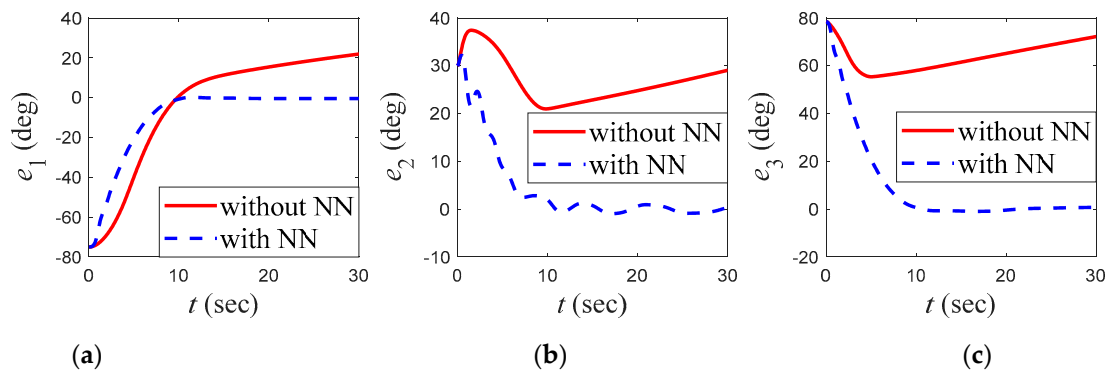


Figure 15. Comparison of angle tracking errors under control laws with or without NN. (a) The first value of the angle tracking errors; (b) The second value of the angle tracking errors; (c) The third value of the angle tracking errors.

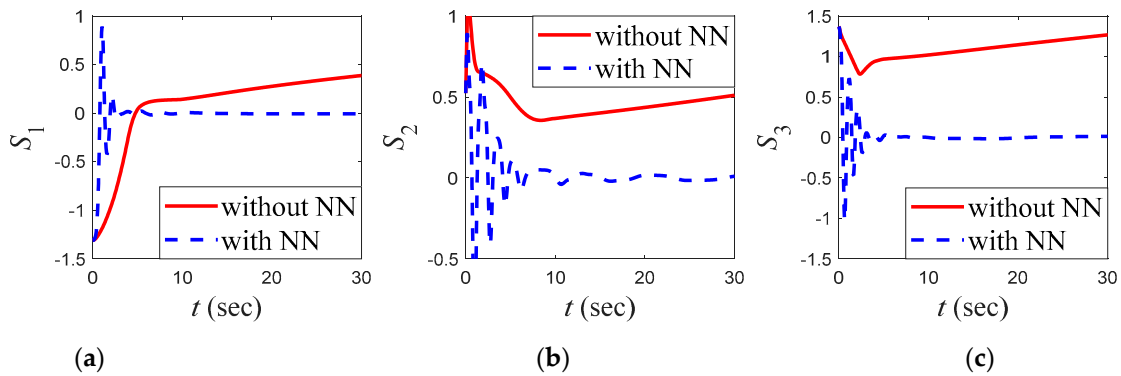


Figure 16. Comparison of sliding manifolds under control laws with or without NN. (a) The first value of the sliding manifold; (b) The second value of the sliding manifold; (c) The third value of the sliding manifold.

Although studies have shown that the use of CMGs as reactionless actuators can reduce the dynamic coupling between the platform and manipulators, the dynamic coupling cannot be eliminated completely because of the existence of inertial forces. The disturbing torque $\tau_{disturb} \in \mathbb{R}^3$ of manipulators to the platform can be calculated by the following function

$$\tau_{disturb} = -(\mathbf{s}_0^\times)^T \dot{\mathbf{v}}_b - \mathbf{I}_0 \dot{\boldsymbol{\omega}}_b - \mathbf{s}_0^\times \boldsymbol{\omega}_b^\times \mathbf{v}_b - \boldsymbol{\omega}_b^\times \mathbf{I}_0 \boldsymbol{\omega}_b - \mathbf{M} \begin{bmatrix} \dot{\mathbf{v}}_b^T \\ \dot{\boldsymbol{\omega}}_b^T \end{bmatrix}^T - \mathbf{F} \quad (61)$$

where $\mathbf{M} \in \mathbb{R}^{3 \times 6}$ and $\mathbf{F} \in \mathbb{R}^3$ are part of the mass matrix \mathbf{M} and the nonlinear generalized inertia forces \mathbf{F}^{It} in Equation (3), respectively. Their relationships are $\mathbf{M} = \mathbf{M}(4 : 6)$ and $\mathbf{F} = \mathbf{F}^{It}(4 : 6)$. We then propose another integrated control scheme with the same ANTSMB controller and inverse dynamic controller but without a controller for the platform, i.e., $\mathbf{f}_b = \boldsymbol{\tau}_b = \mathbf{0}_{3 \times 1}$. Figure 17 shows that the disturbing torque $\tau_{disturb}$ always exists if the platform is not controlled. A comparison of the angle tracking errors under the same control law with or without platform control is illustrated in Figure 18. It is obvious that stabilization control of the platform contributes to improving the tracking accuracy of the manipulator.

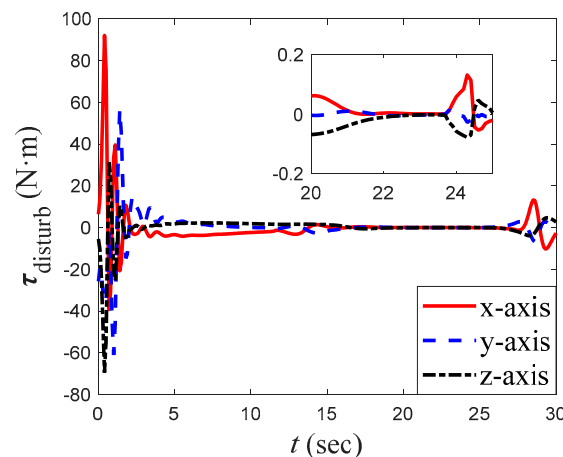


Figure 17. Disturbing torque of manipulators to the platform.

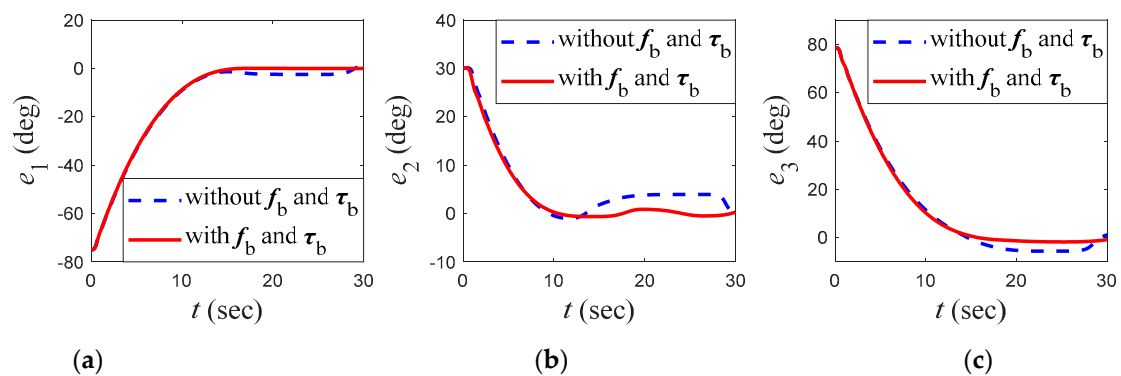


Figure 18. Comparison of angle tracking errors with and without platform control. (a) The first value of the angle tracking error; (b) The second value of the angle tracking error; (c) The third value of the angle tracking error.

6. Conclusions

In this paper, a new integrated control scheme of both the satellite platform stabilization control and the manipulator tracking control is proposed for a reactionless SRS actuated by CMGs. In the tracking control of the manipulator, an ANTSM controller using RBFNN with a new weight adaptive law guarantees finite time convergence of the tracking errors and does not require any prior knowledge of the upper bound of system uncertainties. Both the asymptotic convergence of the ANTSM controller and the uniformly ultimately boundedness of the improved ANTSM controller for practical implementation is strictly proved with a high mathematical standard by the Lyapunov method. Numerical simulation results demonstrate the effectiveness of the proposed controls, indicating that the neural network plays a significant role in increasing control accuracy. Comparative simulations show that the improved ANTSM controller using RBFNN has better performance and robustness, while the platform controller benefits the tracking control of the manipulator in spite of the CMG-actuation. The study provides a new tracking control method for a single-arm or multi-arm space robot, which is suitable for practical implementation. The proposed controller can also be applied to space debris capturing and removal missions.

Author Contributions: All authors were contributed equally. Methodology, X.X. and Y.J.; software, X.X. and Y.J.; writing-original draft, X.X. and Y.J.; writing-review and editing, Y.J., X.W. and J.Z.; funding acquisition, Y.J. and J.Z. All authors have read and agreed to the published version of the manuscript.

Funding: This work is supported by the National Key Research and Development Program of China (Grant No. 2018AAA0103003).

Institutional Review Board Statement: Not applicable.

Informed Consent Statement: Not applicable.

Data Availability Statement: The datasets employed during the current study are available from the corresponding author on request.

Conflicts of Interest: The authors declare that they have no conflict of interest.

References

1. Flores-Abad, A.; Ma, O.; Pham, K.; Ulrich, S. A Review of Space Robotics Technologies for On-Orbit Servicing. *Prog. Aerosp. Sci.* **2014**, *68*, 1–26. [[CrossRef](#)]
2. Jia, S.; Shan, J. Continuous Integral Sliding Mode Control for Space Manipulator with Actuator Uncertainties. *Aerosp. Sci. Technol.* **2020**, *106*, 106192. [[CrossRef](#)]
3. Shan, M.; Guo, J.; Gill, E. Review and Comparison of Active Space Debris Capturing and Removal Methods. *Prog. Aerosp. Sci.* **2016**, *80*, 18–32. [[CrossRef](#)]
4. Palma, P.; Seweryn, K.; Rybus, T. Impedance Control Using Selected Compliant Prismatic Joint in a Free-Floating Space Manipulator. *Aerospace* **2022**, *9*, 406. [[CrossRef](#)]

5. Xia, P.; Luo, J.; Wang, M.; Yuan, J. Constrained Compliant Control for Space Robot Postcapturing Uncertain Target. *J. Aerosp. Eng.* **2019**, *32*, 04018117. [[CrossRef](#)]
6. Chen, G.; Wang, Y.; Wang, Y.; Liang, J.; Zhang, L.; Pan, G. Detumbling Strategy Based on Friction Control of Dual-Arm Space Robot for Capturing Tumbling Target. *Chin. J. Aeronaut.* **2020**, *33*, 1093–1106. [[CrossRef](#)]
7. Hu, Q.; Guo, C.; Zhang, Y.; Zhang, J. Recursive Decentralized Control for Robotic Manipulators. *Aerosp. Sci. Technol.* **2018**, *76*, 374–385. [[CrossRef](#)]
8. Jia, Y.; Misra, A.K. Trajectory Planning for a Space Robot Actuated by Control Moment Gyroscopes. *J. Guid. Control. Dyn.* **2018**, *41*, 1838–1842. [[CrossRef](#)]
9. Feng, X.; Jia, Y.; Xu, S. Dynamics and Momentum Equalization Control of Redundant Space Robot with Control Moment Gyroscopes for Joint Actuation. In Proceedings of the AIAA/AAS Astrodynamics Specialist Conference, Long Beach, CA, USA, 13–16 September 2016.
10. James, F.; Shah, S.V.; Singh, A.K.; Krishna, K.M.; Misra, A.K. Reactionless Maneuvering of a Space Robot in Precapture Phase. *J. Guid. Control Dyn.* **2016**, *39*, 2419–2425. [[CrossRef](#)]
11. Peck, M.; Paluszek, M.; Thomas, S.; Mueller, J. Control-Moment Gyroscopes for Joint Actuation: A New Paradigm in Space Robotics. In Proceedings of the 1st Space Exploration Conference: Continuing the Voyage of Discovery, Orlando, FL, USA, 30 January–1 February 2005.
12. Peck, M. Low-Power, High-Agility Space Robotics. In Proceedings of the AIAA Guidance, Navigation, and Control Conference and Exhibit, San Francisco, CA, USA, 15–18 August 2005.
13. Brown, D. Control Moment Gyros as Space-Robotics Actuators. In Proceedings of the AIAA Guidance, Navigation and Control Conference and Exhibit, Honolulu, HI, USA, 18–21 August 2008.
14. Brown, D.; Peck, M. Energetics of Control Moment Gyroscopes as Joint Actuators. *J. Guid. Control Dyn.* **2009**, *32*, 1871–1883. [[CrossRef](#)]
15. Shen, D.; Tang, L.; Hu, Q.; Guo, C.; Li, X.; Zhang, J. Space Manipulator Trajectory Tracking Based on Recursive Decentralized Finite-Time Control. *Aerosp. Sci. Technol.* **2020**, *102*, 105870. [[CrossRef](#)]
16. Wang, X.; Shi, L.; Katupitiya, J. A Strategy to Decelerate and Capture a Spinning Object by a Dual-Arm Space Robot. *Aerosp. Sci. Technol.* **2021**, *113*, 106682. [[CrossRef](#)]
17. Song, C.; Fei, S.; Cao, J.; Huang, C. Robust Synchronization of Fractional-Order Uncertain Chaotic Systems Based on Output Feedback Sliding Mode Control. *Mathematics* **2019**, *7*, 599. [[CrossRef](#)]
18. Cong, B.; Liu, X.; Chen, Z. Improved Adaptive Sliding Mode Control for a Class of Second-Order Mechanical Systems: Improved Adaptive Sliding Mode Control. *Asian J. Control* **2013**, *15*, 1862–1866. [[CrossRef](#)]
19. Yoo, D.S.; Chung, M.J. A Variable Structure Control with Simple Adaptation Laws for Upper Bounds on the Norm of the Uncertainties. *IEEE Trans. Autom. Control* **1992**, *37*, 860–865. [[CrossRef](#)]
20. Jia, Y.; Xu, S. Decentralized Adaptive Sliding Mode Control of a Space Robot Actuated by Control Moment Gyroscopes. *Chin. J. Aeronaut.* **2016**, *29*, 688–703. [[CrossRef](#)]
21. Jia, Y.; Misra, A.K. Robust Trajectory Tracking Control of a Dual-Arm Space Robot Actuated by Control Moment Gyroscopes. *Acta Astronaut.* **2017**, *137*, 287–301. [[CrossRef](#)]
22. Xu, W.; Qu, S.; Zhao, L.; Zhang, H. An Improved Adaptive Sliding Mode Observer for Middle- and High-Speed Rotor Tracking. *IEEE Trans. Power Electron.* **2021**, *36*, 1043–1053. [[CrossRef](#)]
23. Leeghim, H.; Choi, Y.; Bang, H. Adaptive Attitude Control of Spacecraft Using Neural Networks. *Acta Astronaut.* **2009**, *64*, 778–786. [[CrossRef](#)]
24. Zou, A.-M.; Kumar, K.D. Adaptive Attitude Control of Spacecraft without Velocity Measurements Using Chebyshev Neural Network. *Acta Astronaut.* **2010**, *66*, 769–779. [[CrossRef](#)]
25. Li, J.; Wang, J.; Peng, H.; Zhang, L.; Hu, Y.; Su, H. Neural Fuzzy Approximation Enhanced Autonomous Tracking Control of the Wheel-Legged Robot under Uncertain Physical Interaction. *Neurocomputing* **2020**, *410*, 342–353. [[CrossRef](#)]
26. Zou, A.-M.; Kumar, K.D.; Hou, Z.-G.; Liu, X. Finite-Time Attitude Tracking Control for Spacecraft Using Terminal Sliding Mode and Chebyshev Neural Network. *IEEE Trans. Syst. Man Cybern. B* **2011**, *41*, 950–963. [[CrossRef](#)]
27. Zou, Y. Attitude Tracking Control for Spacecraft with Robust Adaptive RBFNN Augmenting Sliding Mode Control. *Aerosp. Sci. Technol.* **2016**, *56*, 197–204. [[CrossRef](#)]
28. Nafia, N.; El Kari, A.; Ayad, H.; Mjahed, M. Robust Interval Type-2 Fuzzy Sliding Mode Control Design for Robot Manipulators. *Robotics* **2018**, *7*, 40. [[CrossRef](#)]
29. Feng, Y.; Yu, X.; Man, Z. Non-Singular Terminal Sliding Mode Control of Rigid Manipulators. *Automatica* **2002**, *38*, 2159–2167. [[CrossRef](#)]
30. Nojavanzadeh, D.; Badamchizadeh, M. Adaptive Fractional-Order Non-Singular Fast Terminal Sliding Mode Control for Robot Manipulators. *IET Control Theory Appl.* **2016**, *10*, 1565–1572. [[CrossRef](#)]
31. Mohammadi Asl, R.; Shabbouei Hagh, Y.; Palm, R. Robust Control by Adaptive Non-Singular Terminal Sliding Mode. *Eng. Appl. Artif. Intell.* **2017**, *59*, 205–217. [[CrossRef](#)]
32. Abooe, A.; Arefi, M.M.; Sedghi, F.; Abootalebi, V. Robust Nonlinear Control Schemes for Finite-Time Tracking Objective of a 5-DOF Robotic Exoskeleton. *Int. J. Control* **2019**, *92*, 2178–2193. [[CrossRef](#)]

33. Abooe, A.; Hayeri Mehrizi, M.; Arefi, M.M.; Yin, S. Finite-Time Sliding Mode Control for a 3-DOF Fully Actuated Autonomous Surface Vehicle. *Trans. Inst. Meas. Control* **2021**, *43*, 371–389. [[CrossRef](#)]
34. Guo, S.; Li, D.; Meng, Y.; Fan, C. Task Space Control of Free-Floating Space Robots Using Constrained Adaptive RBF-NTSM. *Sci. China Technol. Sci.* **2014**, *57*, 828–837. [[CrossRef](#)]
35. Zhang, S.; Yang, P.; Kong, L.; Chen, W.; Fu, Q.; Peng, K. Neural Networks-Based Fault Tolerant Control of a Robot via Fast Terminal Sliding Mode. *IEEE Trans. Syst. Man Cybern. Syst.* **2019**, *51*, 4091–4101. [[CrossRef](#)]
36. Wang, X. Finite-Time Gradient Descent-Based Adaptive Neural Network Finite-Time Control Design for Attitude Tracking of a 3-DOF Helicopter. *arXiv* **2021**, arXiv:2107.12924.
37. Vijay, M.; Jena, D. Backstepping Terminal Sliding Mode Control of Robot Manipulator Using Radial Basis Functional Neural Networks. *Comput. Electr. Eng.* **2018**, *67*, 690–707. [[CrossRef](#)]
38. Wang, L.; Chai, T.; Zhai, L. Neural-Network-Based Terminal Sliding-Mode Control of Robotic Manipulators Including Actuator Dynamics. *IEEE Trans. Ind. Electron.* **2009**, *56*, 3296–3304. [[CrossRef](#)]
39. Wang, P.; Zhang, D.; Lu, B. Trajectory Tracking Control for Chain-Series Robot Manipulator: Robust Adaptive Fuzzy Terminal Sliding Mode Control with Low-Pass Filter. *Int. J. Adv. Robot. Syst.* **2020**, *17*, 172988142091698. [[CrossRef](#)]
40. Xia, X.; Jia, Y.; Xu, S.; Wang, X. An Adaptive Nonsingular Terminal Sliding Mode Tracking Control Using Neural Networks for Space Manipulators Actuated by CMGs. In Proceedings of the AAS/AIAA Astrodynamics Specialist Conference, Snowbird, UT, USA, 19–23 August 2018; Volume 167, pp. 3185–3198.
41. Wang, X.; Xu, B.; Cheng, Y.; Wang, H.; Sun, F. Robust Adaptive Learning Control of Space Robot for Target Capturing Using Neural Network. *IEEE Trans. Neural Netw. Learn. Syst.* **2022**, 1–11. [[CrossRef](#)]
42. Yan, W.; Liu, Y.; Lan, Q.; Zhang, T.; Tu, H. Trajectory Planning and Low-Chattering Fixed-Time Nonsingular Terminal Sliding Mode Control for a Dual-Arm Free-Floating Space Robot. *Robotica* **2022**, *40*, 625–645. [[CrossRef](#)]
43. Moosavian, S.A.A.; Papadopoulos, E. Free-Flying Robots in Space: An Overview of Dynamics Modeling, Planning and Control. *Robotica* **2007**, *25*, 537–547. [[CrossRef](#)]
44. Hu, Q.; Zhang, J. Dynamics and Trajectory Planning for Reconfigurable Space Multibody Robots. *J. Mech. Des.* **2015**, *137*, 092304. [[CrossRef](#)]
45. Banerjee, A.K. *Flexible Multibody Dynamics: Efficient Formulations and Applications*; John Wiley & Sons, Ltd.: Chichester, UK, 2016.
46. Feng, X.; Jia, Y.; Xu, S. Dynamics of Flexible Multibody Systems with Variable-Speed Control Moment Gyroscopes. *Aerosp. Sci. Technol.* **2018**, *79*, 554–569. [[CrossRef](#)]
47. Huang, P.; Yuan, J.; Liang, B. Adaptive Sliding-Mode Control of Space Robot during Manipulating Unknown Objects. In Proceedings of the 2007 IEEE International Conference on Control and Automation, Guangzhou, China, 30 May–1 June 2007; pp. 2907–2912.
48. Feng, Y.; Yu, X.; Man, Z. Non-Singular Terminal Sliding Mode Control and Its Application for Robot Manipulators. In Proceedings of the the 2001 IEEE International Symposium on Circuits and Systems, Sydney, Australia, 6–9 May 2001; Volume 3, pp. 545–548.
49. Wheeler, G.; Su, C.; Stepanenko, Y. A Sliding Mode Controller with Improved Adaptation Laws for the Upper Bounds on the Norm of Uncertainties. *Automatica* **1998**, *34*, 1657–1661. [[CrossRef](#)]